Journal of Materials Chemistry C

PAPER

View Article Online
View Journal | View Issue

Open Access Article. Published on 25 January 2016. Downloaded on 10/04/2017 04:47:12.
This article is licensed under a Creative Commons Attribution 3.0 Unported Licence.

Cite this: J. Mater. Chem. C, 2016, 4, 3379

SWCNT photocathodes sensitised with InP/ZnS core–shell nanocrystals†

Thomas J. Macdonald,[ab] Daniel D. Tune,[cd] Melissa R. Dewi,[b] Joseph C. Bear,[a] Paul D. McNaughter,[e] Andrew G. Mayes,[e] William M. Skinner,[b] Ivan P. Parkin,[a] Joseph G. Shapter[d] and Thomas Nann*[bf]

Received 17th November 2015,
Accepted 25th January 2016

DOI: 10.1039/c5tc03833b

www.rsc.org/MaterialsC

Increasing the light harvesting efficiency of photocathodes is an integral part of optimising the future efficiencies of solar technologies. In contrast to the more extensively studied photoanode systems, current state-of-the-art photocathodes are less efficient and are commonly replaced with rare and expensive materials such as platinum group metals. The significance of photocathodes is in the development of tandem electrodes, enhancing the performance of existing devices. Carbon nanotubes are promising candidates for photocathodes, which, in addition to their p-type conductivity and catalytic properties, possess a suite of unique optical and electrical attributes. This work describes the fabrication of single walled carbon nanotube (SWCNT) photocathodes sensitised with indium phosphide/zinc sulfide (InP/ZnS) core–shell nanocrystals (NCs). Under air mass (AM) 1.5 conditions, the sensitisation of SWCNT photocathodes with InP/ZnS NCs increased the photocurrent density by 350% of the unsensitised output. This significant enhancement of current density demonstrates the potential of InP/ZnS NCs as effective sensitisers to improve the performance of carbon-based photocathode thin films.

Introduction

The depletion of fossil fuels has encouraged research into renewable energy generation and one focus area is the improvement of light harvesting through the use of tailor made nanomaterials. Optimising the spectral conversion efficiency is an essential part of improving state-of-the-art photovoltaic (PV) and water splitting devices. Quantum size effects in semiconductor nanocrystals (NCs) make them versatile sensitisers for renewable energy generation. As a result of quantum confinement, semiconductor NCs can be tuned by size to enhance exploitation of the solar spectrum.[1,2] Controlling the size of NCs can minimize the spectral losses associated with organic dye molecules by offering a tunable absorption threshold, large redshift, high absorption coefficient and broad absorption spectrum which extends into the UV.[3–5] Additionally, variation of NC size offers different band energies which maximizes photoinduced charge separation and improves the electron transfer process.[6–8]

Indium phosphide (InP), a p-type semiconductor, has been used for water splitting in a variety of nanostructures including: nanopillars,[9] nanowires[10] and NCs.[11,12] InP NCs are one of the most widely studied cadmium-free semiconductor materials for this purpose. The synthesis of monodisperse InP NCs is best achieved using the hot injection method,[13] however other promising synthesis routes have also been proposed.[14,15] Since the properties of NCs are strongly dependent on their dimensions, the synthesis of monodisperse NCs is important for a range of applications including optoelectronic and magnetic storage media.[16] For example, in optical devices the quantum yield and color sharpness is heavily dependent on synthesising NCs with narrow size distributions ($<5\%$).[17,18] The interest in InP NCs continues to grow, due to their p-type conductivity which makes them valuable in a variety of photocathode systems[19,20] and is in contrast to the more commonly employed NCs (such as CdSe), which exhibit n-type conductivity.[21] Compared to the level of development of TiO_2 photoanode studies in the literature, the current efficiency of photocathodes remains somewhat lacking. This is despite the fact that they are, of course, an essential part of many PV systems and water splitting devices that could in theory add significantly to the overall yield of such technologies. It is common practice to use relatively simple catalytic systems based on platinum (Pt) as the cathode material instead.

[a] Department of Chemistry, University College London, London, UK
[b] Ian Wark Research Institute, University of South Australia, South Australia, Australia
[c] Institute of Nanotechnology, Karlsruhe Institute of Technology, Karlsruhe, Germany
[d] Centre for Nanoscale Science and Technology, Flinders University, South Australia, Australia
[e] School of Chemistry, University of East Anglia, Norwich, UK
[f] MacDiarmid Institute for Advanced Materials and Nanotechnology, School of Chemical and Physical Sciences, Victoria University of Wellington, Wellington, New Zealand. E-mail: thomas.nann@vuw.ac.nz

† Electronic supplementary information (ESI) available. See DOI: 10.1039/c5tc03833b

Open Access Article. Published on 25 January 2016. Downloaded on 10/04/2017 04:47:12.
This article is licensed under a Creative Commons Attribution 3.0 Unported Licence.

This is partly due to poor photocathode efficiencies and also because their implementation in devices introduces added levels of design complexity due to the requirement for current matching to the anode. Unfortunately, Pt is a rare material, which means that its use as a cathode will continue to limit commercial applications and alternatives are thus desirable. Oxides of nickel (NiO) and copper (Cu_2O) are widely-used p-type materials for both photovoltaic[22] and water-splitting applications[23] and while NiO is currently the most popular photocathode material,[24–27] a carbon-based substitute would be desirable. Coupled with the p-type conductivity[28] and large variety of carbon nanotubes, thin films of this material offer a promising potential replacement for platinum catalysts and metal oxide based photocathodes.

CNTs can be semiconducting or metallic, depending on the orientation of the graphene lattice with respect to the longitudinal axis. In the case of semiconducting nanotube walls, the bandgap scales inversely with the tube diameter. Multi-walled carbon nanotubes often have dozens of concentric walls and the mixing of states and large diameter of the outermost wall means that the overall nature of the tubes is always metallic. Individual single walled carbon nanotubes (SWCNTs) can be either metallic or semiconducting, but it is difficult to generate exclusively one type in large quantities so the as-produced material is usually a mixture. Films made from such material have both semiconductor-like absorption features as well as metallic-like electrical characteristics.[29] Importantly, the work function of CNTs can be significantly adjusted to tailor their use to different device applications. Methods to modify the work function include chemical doping,[30] intercalation of alkali metals[31] and plasma treatment,[31] and such modification has been found to help facilitate charge separation in the anodes of some PV systems.[28,31] The unique electronic and physical properties of mixed SWCNT films has resulted in their incorporation into dye-sensitised,[32–34] organic[35,36] and solid-state silicon solar cells,[37] and purified semiconducting SWCNTs are receiving increasing attention as the absorbers in novel solar architectures due to their potential to harvest sunlight.[38–41] While advancements in modifying the work function of carbon nanotube films can certainly have positive impacts on their use as photocatalysts and replacements for platinum, their further sensitisation with semiconducting NCs is a new approach that provides the ability to more fully exploit the solar spectrum. While previous work on hybrid CNTNC transistors,[42] conjugate CNT–NCs,[43,44] NC sensitised CNT–TiO_2,[45] CNT–ZnO[46] and silicon[47] systems has been reported, to the best of our knowledge no work has incorporated NCs as sensitisers for standalone CNT photocathodes.

This study investigates the use of SWCNTs as one-dimensional (1D) thin film photocathodes. The photocathodes are prepared by depositing SWCNTs on gold-coated glass substrates. This work uses unsorted, highly carboxylated arc-discharge nanotubes with an average diameter of 1.5 nm (band gap ~0.7 eV) and Fermi level of approximately 4.6–4.7 eV. Monodisperse InP/ZnS NCs with a bandgap around 2.1 eV are used as sensitisers in order to enhance light absorption by the films. InP/ZnS NCs are bound to the surface of SWCNT photocathodes with the assistance of thiol ligands. The proposed energy diagram of the photocathode is illustrated in Fig. 1.

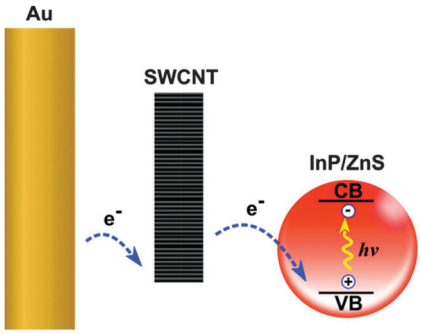

Fig. 1 Proposed photoexcitation of InP/ZnS NCs on SWCNT thin film.

Experimental section

Materials

Trioctylphosphine (technical grade, 90%), trioctylphosphine oxide (technical grade, 90%), 1-octadecene (technical grade, 90%), zinc undecylenate (98%), zinc diethyldithiocarbamate (97%), indium(III) chloride (98%), tris(trimethylsilyl)phosphine (95%) and stearic acid (reagent grade, 95%) were purchased from Sigma Aldrich and used as received. Hexadecylamine (technical grade, 90%) and 1-dodecylphosphonic acid (95%) were purchased from Alfa Aesar and used as received. Laboratory solvents of the highest possible grade were purchased from Fisher Scientific Limited.

Synthesis of InP/ZnS NCs

Indium phosphide QDs were synthesised according to Xu *et al.*[48] Briefly, a nitrogen-purged Schlenk flask was charged with stearic acid (28.5 mg, 0.1 mmol), zinc undecylenate (30 mg, 0.07 mmol), indium(III) chloride (22 mg, 0.1 mmol) and hexadecylamine (48 mg, 0.2 mmol). To this, 1-octadecene (2 ml) was added, and the mixture vacuum/back filled with nitrogen three times before heating to 280 °C. On reaching 280 °C, a solution of tris(trimethylsilyl)phosphine (1 ml, 0.1 M) in 1-octadecene was rapidly injected, and the solution heated at 260 °C for 20 minutes. The flask was then placed in water to cool to room temperature.

For the overgrowth of the ZnS shell onto the InP cores, zinc diethyldithiocarbamate (72 mg, mmol) and zinc undecylenate (100 mg, mmol) were added into the flask containing the cores and vacuum/back filled with nitrogen three times before heating to 180 °C for 10 minutes, increasing to 240 °C for 20 minutes. The flask was then placed in water to cool to room temperature. The InP/ZnS QDs were precipitated with ethanol (~80 ml) and isolated by centrifugation (5 minutes at 3000 × g). The QDs were washed twice with ethanol (2 × 60 ml) to remove any unbound surfactants, and dispersed in *n*-hexane (10 ml).

Characterisation

Optical absorption spectroscopy of InP/ZnS NCs was carried out on an Agilent Cary 300 spectrometer. Photoluminescence spectroscopy,

 This journal is © The Royal Society of Chemistry 2016

Open Access Article. Published on 25 January 2016. Downloaded on 10/04/2017 04:47:12.
This article is licensed under a Creative Commons Attribution 3.0 Unported Licence.

quantum yield and lifetime measurements were carried out on an Edinburgh Instruments Fluorimeter FLS980. TEM was performed on a JEOL JEM-2100F with an acceleration voltage of 200 kV. Where appropriate, XRD was carried out using a Scintag ARL X'tra diffractometer (using Cu-radiation). SEM images were obtained with a Ziess MERLIN. XPS measurements were taken using monochromatized Al Kα X-rays (300 W) in a Kratos Axis-Ultra spectrometer (10 eV analyzer pass energy). The time of flight secondary ion mass spectroscopy (ToF-SIMS) instrument was a Physical Electronics TRIFT V NanoToF. Depth profiles were conducted using a single Au 30 keV LMIG source operating in pulsed and continuous modes for analysis and sputtering cycles respectively.

Preparation of SWCNT solutions

Arc-discharge nanotubes (P3-SWNT, Carbon Solution Inc, California, USA) were suspended in 1% aqueous TritonX-100 (Sigma, Australia) by bath sonication for 1 h, then centrifuged (10 000 g, 30 min) and the supernatant was collected.

Preparation of SWCNT photocathodes

Gold coated glass slides (AU.0100.ALSI, Platypus®) were washed with acetone, isopropanol and DI water before being suspended in a piranha solution for 45 seconds. SWCNT thin films were then deposited as described previously.[49,50] Briefly, the nanotube solution was filtered through mixed cellulose ester (MCE) membranes (0.45 μm, HAWP, Millipore Australia) and rinsed with copious Di water. The filter was placed nanotube side down on the gold surface then compressed and baked (100 °C, 20 min). Upon cooling, the entire substrate was immersed in an acetone bath (30 min) to dissolve the MCE membrane. After a further two baths in clean acetone the bare SWCNT film was left on the gold coated glass substrate.

Sensitising the SWCNT photocathodes

Finally, SWCNT photocathodes were sensitised with InP/ZnS NCs by doing 5 sequential depositions of NCs by drop casing, allowing the solvent (hexane) to evaporate in-between depositions. The NC sensitised photocathodes were gently washed with DI water to remove any unbound particulates from the surface.

Current density measurements

The SWCNT photocathodes had an area of 1 cm^2 and were illuminated with 100 mW cm^{-2} of light from a xenon-arc source passing through an AM1.5G filter (Abet Technologies) at ambient temperature. The plane of illumination was calibrated with a monocrystalline silicon reference cell (91150V, Newport). Spectro-electrochemical measurements were carried out using a PG 310 potentiostat (HEKA Electronics). Current density measurements were performed using a Teflon photoelectrochemical cell consisting of a Pt counter electrode, a Ag/AgCl 3 M KCl reference electrode and a SWCNT working photocathode. Photocathodes were illuminated with light–dark cycles of 30 seconds for 5 minutes.

Results

Spectroscopy of InP/ZnS NCs

InP/ZnS NCs were prepared by a method previously described.[48] InP NCs were shelled with ZnS to increase the stability and quantum yield. The resulting core–shell NCs were characterized using optical absorption and photoluminescence (PL) spectroscopies. Fig. 2 shows the absorbance and emission spectra. The absorbance spectrum shows an excitonic peak at 472 nm, whilst the emission spectrum shows a strong peak at 575 nm, with full width at half maximum (FWHM) of 90 nm.[48,51] Where appropriate, the PL measurements were carefully controlled using an integrating sphere. Under these controlled conditions, the PL quantum yield of the InP core NCs was calculated to be 13%, and this was increased to 21% after shelling with ZnS. The PL lifetimes of the NCs were fitted with a stretched exponential[52] (eqn (1)) and calculated to be 58 ± 0.38 ns, β 0.88 ± 0.06. These values were consistent with our previous report for InP/ZnS NCs showing similar optical properties.[53] Fig. S1 of the ESI† shows the absorption and PL spectroscopy of the bare InP core NCs. The values obtained from the measurements of both the core and the core–shell structures are tabulated in Table S1 of the ESI.† To help clarify the physical properties of the InP/ZnS NCs, the band gap was calculated from the emission spectra to be ~2.10 eV and this was further verified from the Tauc plot of the absorption, inset in Fig. 2. This was important in order to help describe the charge transfer pathway from the SWCNTs to the NCs as described in Fig. 1.

$$I = I_0 + A\exp\left(\frac{-t}{\tau}\right)^{\beta}. \quad (1)$$

TEM and SEM

Fig. 3 shows transmission electron microscope (TEM) images of InP/ZnS NCs. The NCs were found to have an average particle size of 2.40 ± 0.80 nm, which is consistent with our previous reports for InP/ZnS NCs.[48,53] Particle sizes were calculated using ImageJ software and verified by dynamic light scattering. Fig. S2 in the ESI† shows the particle size frequency distribution and hydrodynamic diameters from DLS. Fig. 3(a) shows the NCs

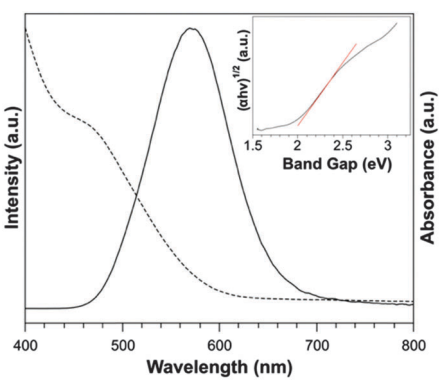

Fig. 2 Absorbance (dashed line) and emission (solid line) spectra for InP/ZnS NCs. The inset shows a Tauc plot absorption spectrum for band gap estimation.

Open Access Article. Published on 25 January 2016. Downloaded on 10/04/2017 04:47:12.
This article is licensed under a Creative Commons Attribution 3.0 Unported Licence.

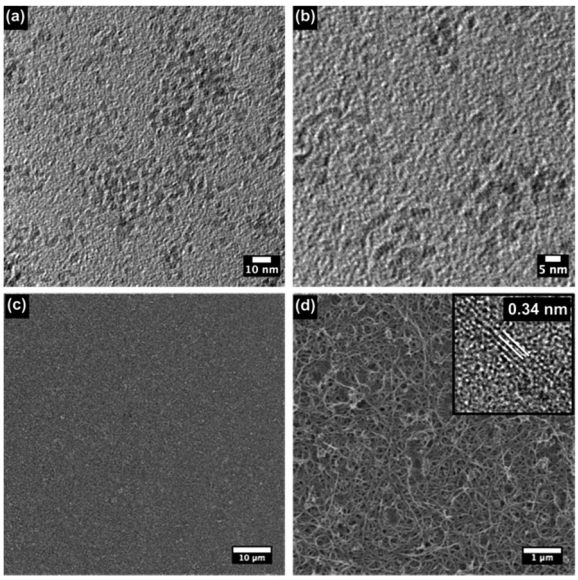

Fig. 3 (a) TEM image of InP/ZnS NCs, (b) HRTEM of InP/ZnS NCs, (c) SEM showing overview of SWCNT photocathodes, (d) magnified SEM showing the network of SWCNTs. The inset shows the lattice fringes of the SWCNTs as measured with TEM.

to have a narrow particle size distribution and slightly irregular shape tending towards spherical. HRTEM confirming the size of the InP/ZnS NCs is shown in Fig. 3(b). For further analysis, ZnS shelling of the InP NCs was characterized using X-ray diffraction (XRD). Fig. S3 in the ESI† shows the XRD patterns for InP/ZnS NCs consistent with the cubic crystal structure of ZnS.[54]

Scanning electron microscope (SEM) images of the SWCNT photocathodes illustrate good overall surface coverage (Fig. 3(c)) as well as allowing estimation of the size of the bundles to be ~40 nm (Fig. 3(d)). The SWCNTs are randomly distributed and highly interwoven to form a nanoporous network that provides both a high surface area to support the NCs, as well as easy access to interior spaces allowing for fast electrolyte diffusion. HRTEM of the SWCNTs was carried out to allow measurement the lattice spacing (Fig. 3(d), inset, with full scale image in Fig. S4, ESI†) which was found to be 0.34 nm consistent with previous reports.[55]

XPS and ToF-SIMS

Fig. 4 shows the X-ray photoelectron spectroscopy (XPS) measurements, which were performed to study the chemical state of the InP/ZnS NCs bound to SWCNT photocathodes. The full survey spectrum is shown in Fig. 4(a) indicating the presence of indium, phosphorus, zinc, sulfur, oxygen and carbon. The atomic compositions are shown in the inset of Fig. 4(a) and are consistent with previous reports of InP/ZnS NCs.[53] The In 3d peaks are shown in Fig. 4(b), with In $3d_{5/2}$ and In $3d_{1/2}$ at 445 eV and 452.6 eV respectively. The In 3d peaks show a spin–orbit splitting of 7.6 eV which, from previous reports,[56,57] is indicative of In(III). The Zn 2p spectrum is shown in Fig. 4(c), and is split into Zn $2p_{3/2}$ (1021.8 eV) and Zn 2p (1044.9 eV) peaks with a separation of 23.1 eV. This can be assigned to Zn(II), again consistent with

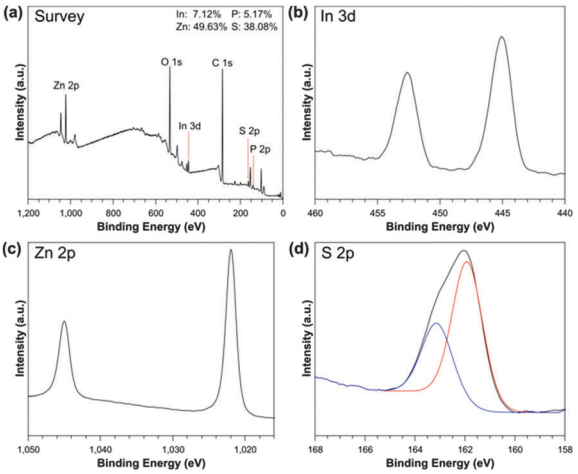

Fig. 4 XPS representing the (a) survey spectra of InP/ZnS NCs, (b) high resolution of In 3d, (c) Zn 2p and (d) S 2p spectra.

previous reports.[56,58] Fig. 4(d) shows the S 2p spectrum, where the fit result suggests a single sulfur environment, being consistent with ZnS, with S $2p_{3/2}$ located at a binding energy of 162.1 eV.[27,59]

Time-of-flight secondary ion mass spectroscopy (ToF-SIMS) provided an alternative verification of the presence of InP/ZnS in the SWCNT photocathode and the depth profile implied by the variation of the counts with sputter time indicates the NCs are rich in Zn ions close to the surface (Fig. S5 of the ESI†).

Photo-electrochemical measurements

To investigate the photocatalytic activity of the SWCNT thin films, the photocurrent density as a function of time was recorded using a three-electrode system and the results are shown in Fig. 5. The system consisted of a Ag|AgCl reference electrode, Pt counter electrode and phosphate-buffered saline (PBS) electrolyte. No external bias was applied between the working and reference electrode for the measurements (an applied potential of 0 V). Fig. 5 shows light–dark cycles over a period of 5 minutes and shows a light-generated current over 30 second intervals. Bare SWCNT films (black line) produced a cathodic photocurrent density of 0.2 μA cm^{-2} under AM 1.5 conditions, confirming the p-type conductivity of the electrode. After sensitisation with InP/ZnS NCs, the maximum current density was increased to 0.7 μA cm^{-2}. Therefore, SWCNT films sensitised with InP/ZnS NCs improved the current density by a factor of 3.5. As a control, our previous work described an InP sensitised gold photocathode,[11] which illustrated photocurrents of 0.1 μA cm^{-2}, significantly lower than the work described here.

In order to test the stability of our NC-sensitised SWCNT photoelectrodes, additional measurements were performed over 1 hour (Fig. S6, ESI†). During this period, light–dark cycles with 5 minute intervals show a consistent photocurrent of the sensitised SWCNT nanophotocathodes. While some drift is present, our system illustrates minimal photocurrent degradation of the NCs over the 1 hour time period. Our results demonstrate that a nanophotocathode can be fabricated from SWCNTs and

 This journal is © The Royal Society of Chemistry 2016

Open Access Article. Published on 25 January 2016. Downloaded on 10/04/2017 04:47:12.
This article is licensed under a Creative Commons Attribution 3.0 Unported Licence.

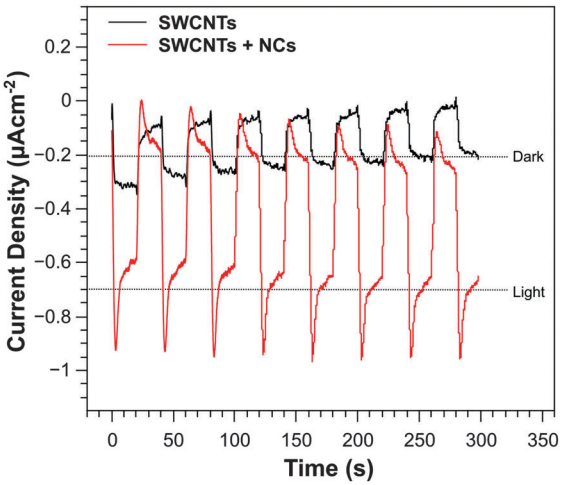

Fig. 5 Current density *vs.* time measurements for SWCNTs with (red) and without (black) InP/ZnS NCs. Measurements for light–dark generated cycles are shown over 5 minutes with 30 second intervals.

adding InP/ZnS NCs can enhance its performance. Similar systems have been reported to produce hydrogen (H_2) gas from water electrolysis, however no H_2 was detected and this was attributed to the low current density.

Further work will focus on improving the experimental setup to allow quantitative assessment of the electrode performance.

Conclusions

This work shows that InP/ZnS NCs can be used as sensitisers for SWCNT photocathodes. The addition of the NCs to the surface of the nanotubes improves the light harvesting capability of SWCNT photocathodes by 350%. The NCs and composite photocathodes were characterized using spectroscopy, TEM, SEM, XRD, XPS, ToF-SIMS and spectro-electrochemical measurements. It was found that the SWCNT photocathodes sensitised with InP/ZnS NCs achieved a current density of 0.70 μA cm^{-2} compared to 0.2 μA cm^{-2} without the NCs.

Acknowledgements

This work was performed in part at the South Australian node of the Australian National Fabrication Facility (ANFF), a company established under the National Collaborative Research Infrastructure Strategy to provide nano and micro-fabrication facilities for Australia's researchers.

References

1 A. P. Alivisatos, *Science*, 1996, **271**, 933–937.
2 V. I. Klimov, A. A. Mikhailovsky, S. Xu, A. Malko, J. A. Hollingsworth, C. A. Leatherdale, H.-J. Eisler and M. G. Bawendi, *Science*, 2000, **290**, 314–317.
3 K. Barnham, J. Luis Marques, J. Hassard and P. O'Brien, *Appl. Phys. Lett.*, 2000, **76**, 1197.
4 V. I. Klimov, S. A. Ivanov, J. Nanda, M. Achermann, I. Bezel, J. A. McGuire and A. Piryatinski, *Nature*, 2007, **447**, 441–446.
5 U. Resch-Genger, M. Grabolle, S. Cavaliere-Jaricot, R. Nitschke and T. Nann, *Nat. Methods*, 2008, **5**, 763–775.
6 L. E. Brus, *J. Chem. Phys.*, 1983, **79**, 5566.
7 L. E. Brus, *J. Chem. Phys.*, 1984, **80**, 4403.
8 P. V. Kamat, *J. Phys. Chem. C*, 2008, **112**, 18737–18753.
9 M. H. Lee, K. Takei, J. Zhang, R. Kapadia, M. Zheng, Y.-Z. Chen, J. Nah, T. S. Matthews, Y.-L. Chueh, J. W. Ager and A. Javey, *Angew. Chem., Int. Ed.*, 2012, **51**, 10760–10764.
10 L. Gao, Y. Cui, J. Wang, A. Cavalli, A. Standing, T. T. T. Vu, M. A. Verheijen, J. E. M. Haverkort, E. P. A. M. Bakkers and P. H. L. Notten, *Nano Lett.*, 2014, **14**, 3715–3719.
11 T. Nann, S. K. Ibrahim, P.-M. Woi, S. Xu, J. Ziegler and C. J. Pickett, *Angew. Chem., Int. Ed.*, 2010, **49**, 1574–1577.
12 S. Chandrasekaran, T. J. Macdonald, Y. J. Mange, N. H. Voelcker and T. Nann, *J. Mater. Chem. A*, 2014, **2**, 9478–9481.
13 S. Xu, S. Kumar and T. Nann, *J. Am. Chem. Soc.*, 2006, **128**, 1054–1055.
14 L. Li and P. Reiss, *J. Am. Chem. Soc.*, 2008, **130**, 11588–11589.
15 M. D. Tessier, D. Dupont, K. De Nolf, J. De Roo and Z. Hens, *Chem. Mater.*, 2015, **27**, 4893–4898.
16 J. Park, K. An, Y. Hwang, J.-G. Park, H.-J. Noh, J.-Y. Kim, J.-H. Park, N.-M. Hwang and T. Hyeon, *Nat. Mater.*, 2004, **3**, 891–895.
17 A. L. Rogach, D. V. Talapin, E. V. Shevchenko, A. Kornowski, M. Haase and H. Weller, *Adv. Funct. Mater.*, 2002, **12**, 653–664.
18 T. J. Macdonald and T. Nann, *Nanomaterials*, 2011, **1**, 79–88.
19 H. M. Chen, C. K. Chen, C. C. Lin, R.-S. Liu, H. Yang, W.-S. Chang, K.-H. Chen, T.-S. Chan, J.-F. Lee and D. P. Tsai, *J. Phys. Chem. C*, 2011, **115**, 21971–21980.
20 S. Chandrasekaran, T. J. Macdonald, A. R. Gerson, T. Nann and N. H. Voelcker, *ACS Appl. Mater. Interfaces*, 2015, 17381–17387.
21 D. Yu, C. Wang and P. Guyot-Sionnest, *Science*, 2003, **300**, 1277–1280.
22 A. Nattestad, M. Ferguson, R. Kerr, Y.-B. Cheng and U. Bach, *Nanotechnology*, 2008, **19**, 295304.
23 A. Paracchino, V. Laporte, K. Sivula, M. Grätzel and E. Thimsen, *Nat. Mater.*, 2011, **10**, 456–461.
24 A. Nattestad, A. J. Mozer, M. K. R. Fischer, Y.-B. Cheng, A. Mishra, P. Bauerle and U. Bach, *Nat. Mater.*, 2010, **9**, 31–35.
25 T. J. Macdonald, J. Xu, S. Elmas, Y. J. Mange, W. M. Skinner, H. Xu and T. Nann, *Nanomaterials*, 2014, **4**, 256–266.
26 H. Tian, B. Xu, H. Chen, E. M. J. Johansson and G. Boschloo, *ChemSusChem*, 2014, **7**, 2150–2153.
27 T. J. Macdonald, Y. J. Mange, M. R. Dewi, H. U. Islam, I. P. Parkin, W. M. Skinner and T. Nann, *J. Mater. Chem. A*, 2015, **3**, 13324–13331.
28 L. Hu, D. S. Hecht and G. Grüner, *Chem. Rev.*, 2010, **110**, 5790–5844.
29 D. Tune and J. Shapter, *Nanomaterials*, 2013, **3**, 655–673.
30 U. Dettlaff-Weglikowska, V. Skákalová, R. Graupner, S. H. Jhang, B. H. Kim, H. J. Lee, L. Ley, Y. W. Park, S. Berber, D. Tománek and S. Roth, *J. Am. Chem. Soc.*, 2005, **127**, 5125–5131.
31 Z. Jijun, H. Jie and L. Jian. P, *Phys. Rev. B: Condens. Matter Mater. Phys.*, 2002, **65**, 193101.

Open Access Article. Published on 25 January 2016. Downloaded on 10/04/2017 04:47:12.
This article is licensed under a Creative Commons Attribution 3.0 Unported Licence.

32 D. D. Tune, B. S. Flavel, J. S. Quinton, A. V. Ellis and J. G. Shapter, *Sol. Energy Mater. Sol. Cells*, 2010, **94**, 1665–1672.
33 T. J. Macdonald, D. D. Tune, M. R. Dewi, C. T. Gibson, J. G. Shapter and T. Nann, *ChemSusChem*, 2015, **8**, 3396–3400.
34 M. Batmunkh, M. J. Biggs and J. G. Shapter, *Small*, 2015, **11**, 2963–2989.
35 M. W. Rowell, M. A. Topinka, M. D. McGehee, H.-J. Prall, G. Dennler, N. S. Sariciftci, L. Hu and G. Gruner, *Appl. Phys. Lett.*, 2006, **88**, 233506.
36 T. P. Tyler, R. E. Brock, H. J. Karmel, T. J. Marks and M. C. Hersam, *Adv. Energy Mater.*, 2011, **1**, 785–791.
37 D. D. Tune, B. S. Flavel, R. Krupke and J. G. Shapter, *Adv. Energy Mater.*, 2012, **2**, 1043–1055.
38 D. J. Bindl, M.-Y. Wu, F. C. Prehn and M. S. Arnold, *Nano Lett.*, 2011, **11**, 455–460.
39 R. M. Jain, R. Howden, K. Tvrdy, S. Shimizu, A. J. Hilmer, T. P. McNicholas, K. K. Gleason and M. S. Strano, *Adv. Mater.*, 2012, **24**, 4436–4439.
40 D. D. Tune and J. G. Shapter, *Energy Environ. Sci.*, 2013, **6**, 2572–2577.
41 M. Gong, T. A. Shastry, Y. Xie, M. Bernardi, D. Jasion, K. A. Luck, T. J. Marks, J. C. Grossman, S. Ren and M. C. Hersam, *Nano Lett.*, 2014, **14**, 5308–5314.
42 C. Biswas, H. Jeong, M. S. Jeong, W. J. Yu, D. Pribat and Y. H. Lee, *Adv. Funct. Mater.*, 2013, **23**, 3653–3660.
43 G. G. Wildgoose, E. J. Lawrence, J. C. Bear and P. D. McNaughter, *Electrochem. Commun.*, 2011, **13**, 1139–1142.
44 J. C. Bear, P. D. McNaughter, K. Jurkschat, A. Crossley, L. Aldous, R. G. Compton, A. G. Mayes and G. G. Wildgoose, *J. Colloid Interface Sci.*, 2012, **383**, 110–117.
45 W. Lee, J. Lee, S. K. Min, T. Park, W. Yi and S.-H. Han, *Mater. Sci. Eng., B*, 2009, **156**, 48–51.
46 J. Chen, C. Li, D. W. Zhao, W. Lei, Y. Zhang, M. T. Cole, D. P. Chu, B. P. Wang, Y. P. Cui, X. W. Sun and W. I. Milne, *Electrochem. Commun.*, 2010, **12**, 1432–1435.
47 V. Švrček, D. Mariotti, T. Nagai, Y. Shibata, I. Turkevych and M. Kondo, *J. Phys. Chem. C*, 2011, **115**, 5084–5093.
48 S. Xu, J. Ziegler and T. Nann, *J. Mater. Chem.*, 2008, **18**, 2653–2656.
49 Z. Wu, Z. Chen, X. Du, J. M. Logan, J. Sippel, M. Nikolou, K. Kamaras, J. R. Reynolds, D. B. Tanner, A. F. Hebard and A. G. Rinzler, *Science*, 2004, **305**, 1273–1276.
50 D. D. Tune, A. J. Blanch, R. Krupke, B. S. Flavel and J. G. Shapter, *Phys. Status Solidi A*, 2014, **211**, 1479–1487.
51 E. Ryu, S. Kim, E. Jang, S. Jun, H. Jang, B. Kim and S.-W. Kim, *Chem. Mater.*, 2009, **21**, 573–575.
52 M. Röding, S. J. Bradley, M. Nydén and T. Nann, *J. Phys. Chem. C*, 2014, **118**, 30282–30290.
53 J. C. Bear, N. Hollingsworth, A. Roffey, P. D. McNaughter, A. G. Mayes, T. J. Macdonald, T. Nann, W. H. Ng, A. J. Kenyon, G. Hogarth and I. P. Parkin, *Adv. Opt. Mater.*, 2015, **3**, 704–712.
54 F. Zan and J. Ren, *J. Mater. Chem.*, 2012, **22**, 1794–1799.
55 A. Kis, G. Csanyi, J.-P. Salvetat, T.-N. Lee, E. Couteau, A. J. Kulik, W. Benoit, J. Brugger and L. Forro, *Nat. Mater.*, 2004, **3**, 153–157.
56 H. Shen, H. Yuan, F. Wu, X. Bai, C. Zhou, H. Wang, T. Lu, Z. Qin, L. Ma and L. S. Li, *J. Mater. Chem.*, 2012, **22**, 18623–18630.
57 Q. Li, C. Zou, L. Zhai, L. Zhang, Y. Yang, X. 'an Chen and S. Huang, *CrystEngComm*, 2013, **15**, 1806–1813.
58 A. Singh, H. Geaney, F. Laffir and K. M. Ryan, *J. Am. Chem. Soc.*, 2012, **134**, 2910–2913.
59 C. A. Prestidge, W. M. Skinner, J. Ralston and R. S. Smart, *Appl. Surf. Sci.*, 1997, **108**, 333–344.

This journal is © The Royal Society of Chemistry 2016